ELSEVIER

Contents lists available at ScienceDirect

Materials Today Communications

journal homepage: www.elsevier.com/locate/mtcomm





Effects of grain size and crystal orientation on tensile properties of pure titanium thin wires

Junji Sakamoto * D, Naoya Tada, Takeshi Uemori

Faculty of Environmental, Life, Natural Science and Technology, Okayama University, 3-1-1 Tsushima-naka, Okayama, Kita-ku 700-8530, Japan

ARTICLE INFO

Keywords: Tensile properties Pure titanium Thin wire Slip deformation Grain size Crystal orientation Cross-section

ABSTRACT

To clarify the effects of the grain size and crystal orientation on the tensile properties of pure titanium thin wires, tensile and stepwise tensile tests were conducted on pure titanium wires with diameters of approximately $180 \, \mu m$ and different average grain sizes (52, 37, 23, and 3.8 μm). When the grain size was large, the fracture strain was significantly smaller, the variation in tensile strength was larger, and the grain size threshold for such properties was a grain-size ratio to wire diameter of 0.13 or greater. For larger grain sizes, the slip system with the highest modified Schmid factor (*MSF*), which is the Schmid factor divided by the critical resolved shear stress of each slip system, was activated in all 15 grains whereas for smaller grain sizes, the percentage of slip systems activated with the highest *MSF* was slightly lower. In addition, the fracture location in a thin wire with larger grain sizes was highly correlated with the average *MSF* of the grains in the cross-section.

1. Introduction

Pure titanium has excellent mechanical properties, corrosion resistance, and biocompatibility, and thin Ti wires have been used in medical devices [1,2]. From the viewpoint of reducing the mental and physical stress on patients undergoing minimally invasive treatment, the need for downsizing medical devices has been increasing in recent years, and materials with sufficient long-term reliability even in small-sized devices are required.

As the number of grains present in the cross-section of a small polycrystalline material decreases, its deformation differs from those of the bulk material [3]. Research focusing on the ratio of sheet thickness to grain size in thin sheet materials has been conducted for aluminum, copper, iron [4], nickel [5], nickel-based superalloys [6], titanium alloy [7], and pure titanium [7–14]. Regarding thin wires, $d_{\rm ave}/D$, the ratio of the average grain size ($d_{\rm ave}$) to the wire diameter (D) is large, the tensile and compressive deformation behaviors are different from those of bulk materials, as reported for stainless steel [15,16], pure nickel [17–19], silver [20,21], and pure titanium [22]. For increasing $d_{\rm ave}/D$, the underlying reason is not simply the decrease in yield stress obtained from the Hall–Petch law [23,24] (owing to increase in grain size), but also the decrease in work hardening owing to the increase in the fraction of grains facing the free surface [15–17]. Fu et al. [15] calculated the surface grain fraction ($f_{\rm s}$) using the number of grains across the diameter

(n) and proposed a relationship between f_s and the macroscopic flow stress. Wang et al. [17] formulated a relationship between the ratio of grain size to the wire diameter and grain boundary density, and used it to indicate the relationship with macroscopic flow stress. In addition to the grain size, the ratio of grain size to the wire diameter should be considered to better understand the deformation behavior of thin wires.

Research on pure titanium has been reported, including analytical studies investigating deformation behavior using crystal plasticity finite element analysis [25–27] and molecular dynamics simulations [28], and experimental studies focusing on crystal orientation [29–39]. The focus on crystal orientation is because pure titanium has a hexagonal-close-packed structure, and the critical resolved shear stress (τ_{CRSS}) differs for each slip system. Although the reported values of τ_{CRSS} vary for pure titanium owing to differences in the chemical composition and other factors, the τ_{CRSS} of each slip system is known to be different. Therefore, the influence of the crystal orientation on the tensile properties probably plays an essential role.

In this study, we conducted tensile and stepwise tensile tests of pure titanium thin wires with different average grain sizes in order to clarify the effects of grain size and crystal orientation on the tensile properties of pure titanium thin wires. In addition to the investigation of macroscopic tensile properties, the slip system activated in a grain and the fracture location in a thin wire were examined considering grain size and crystal orientation.

E-mail address: sakamoto-junji@okayama-u.ac.jp (J. Sakamoto).

^{*} Corresponding author.

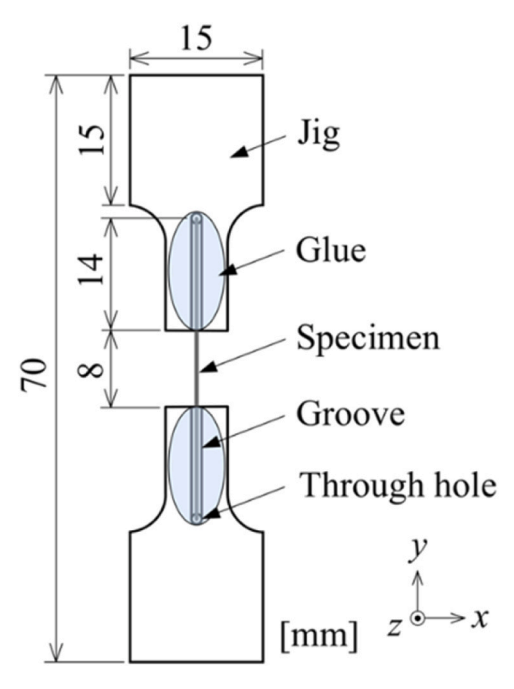


Fig. 1. Shape and size of the specimen and jigs for the tensile test.

2. Material and methods

2.1. Material

Four types of specimens with different average grain sizes were prepared by annealing pure thin Ti wires with a diameter of 200 μm . Titanium is extremely sensitive to oxygen ingress at high temperatures and is particularly prone to embrittlement [7,40]. Therefore, annealing was performed in a vacuum at 1143, 1043, 943, and 843 K. After annealing, the top 10 μm surface layers of the specimens were electropolished to smooth their surfaces. The D value after electropolishing was approximately 180 μm . Electron backscatter diffraction (EBSD) was conducted to determine the grain size and crystal orientation of the specimens. For the EBSD analysis, the sample was analyzed by tilting it by 70° using a scanning electron microscope (SEM), which was then corrected in the software. Normally, the correction is performed by assuming a flat sample. Therefore, an additional correction is required when the surface is curved, as in the case of thin wires. Therefore, the method reported in Ref. [22] was used for correction.

2.2. Tensile test method

Fig. 1 shows the shape and size of the specimen and jigs used for the tensile test. As shown in Fig. 1, the stainless steel jigs were adhered to both ends of an electropolished pure titanium thin wire such that the distance between the jigs was 8 mm. The jigs were bonded using cyanoacrylate adhesive. Tensile tests were carried out using an electromagnetic-force micromaterial-testing machine (MMT-100NB-10, Shimadzu Corp.) at a stroke speed of 0.001 mm/s until the specimen ruptured. During the test, the distance between the jigs (initially 8 mm as shown in Fig. 1) was measured using a measurement instrument (TM-X5040, Keyence Corp.) and the strain was calculated based on the distance. The maximum load in the tensile tests conducted in this study was

10.3 N. Assuming the glue around the specimen was loaded uniformly, the shear stress was 1.30 MPa. Since the shear strength of the glue is 22 MPa or higher, the glue did not peel off, and its deformation was negligible. Three specimens were used for each of the four types.

2.3. Stepwise tensile test method

Specimens were placed in a custom-made tensile test machine reported in the previous paper [22] and subjected to stepwise tensile loading. Stepwise tensile tests were conducted using one specimen each that was annealed at 1143 and 943 K. Table 1 lists the strains calculated using the displacement measurement jigs. Fracture was observed at the 8th step in both specimens. The crystal orientations of the specimens were analyzed using EBSD before the test, and the specimens were observed using SEM at each step of the test.

To clarify the effects of the grain size and crystal orientation on slip deformation, the grain size and modified Schmid factor (*MSF*) of each grain were calculated as follows. First, the grain size of each grain was calculated using Eq. (1),

$$d = \sqrt{S} \tag{1}$$

where S denotes the area within the observed region of each grain. The Schmid factor (SF) and MSF were calculated as

$$SF = \cos \phi \cos \lambda$$
 (2)

$$MSF = \frac{SF}{\tau_{CDSS}} \tag{3}$$

where ϕ and λ in Eq. (2) are the angles between the slip plane normal and tensile directions and between the slip and tensile directions, respectively. In Eq. (3), τ_{CRSS} is the critical resolved shear stress, and the values of τ_{CRSS} for each slip system were listed in Table 2, based on the results of Warwick et al. [33]. The reasons for selecting τ_{CRSS} in Ref. [33] are described in the previous paper [22].

To investigate the interaction between the grains, the geometric compatibility factor m' [40] and N factor [41] were calculated using Eqs. (4) and (5), respectively,

$$m' = (\mathbf{s}_{A} \cdot \mathbf{s}_{B})(\mathbf{n}_{A} \cdot \mathbf{n}_{B}) \tag{4}$$

$$N = (\mathbf{s}_{A} \cdot \mathbf{s}_{B})(\mathbf{n}_{A} \cdot \mathbf{n}_{B}) + (\mathbf{s}_{A} \cdot \mathbf{n}_{B})(\mathbf{n}_{A} \cdot \mathbf{s}_{B})$$
(5)

where s and n are the unit vector in the slip direction and the unit normal vector of the slip plane, respectively. The subscripts A and B represent the slip systems of adjacent grains. Both m' and N assume values between -1 and 1. For a larger value of m', the slip planes and slip directions of the adjacent grains are closely aligned, and for a larger value of N, the shear stress between them is close. This study focuses on the relationship between the initial microstructure and deformation. The aforementioned SF, MSF, m', N values were calculated from the crystal

Table 2 Values of τ_{CRSS} .

Slip system	$ au_{ ext{CRSS}}$ [MPa]
Prismatic <a>	80
Basal <a>	90
Pyramidal <a>	110
Pyramidal <c+a></c+a>	260

Table 1 Estimated strain of stepwise tensile tests.

Step	0th	1st	2nd	3rd	4th	5th	6th	7th	8th
Strain, $d_{\text{ave}}/D = 0.29$	0	0.004 0.005	0.008 0.01	0.012 0.015	0.016 0.02	0.02 0.03	0.03 0.04	0.04 0.05	0.05 0.06
Strain, $d_{\text{ave}}/D = 0.13$	U	0.003	0.01	0.013	0.02	0.03	0.04	0.03	0.00

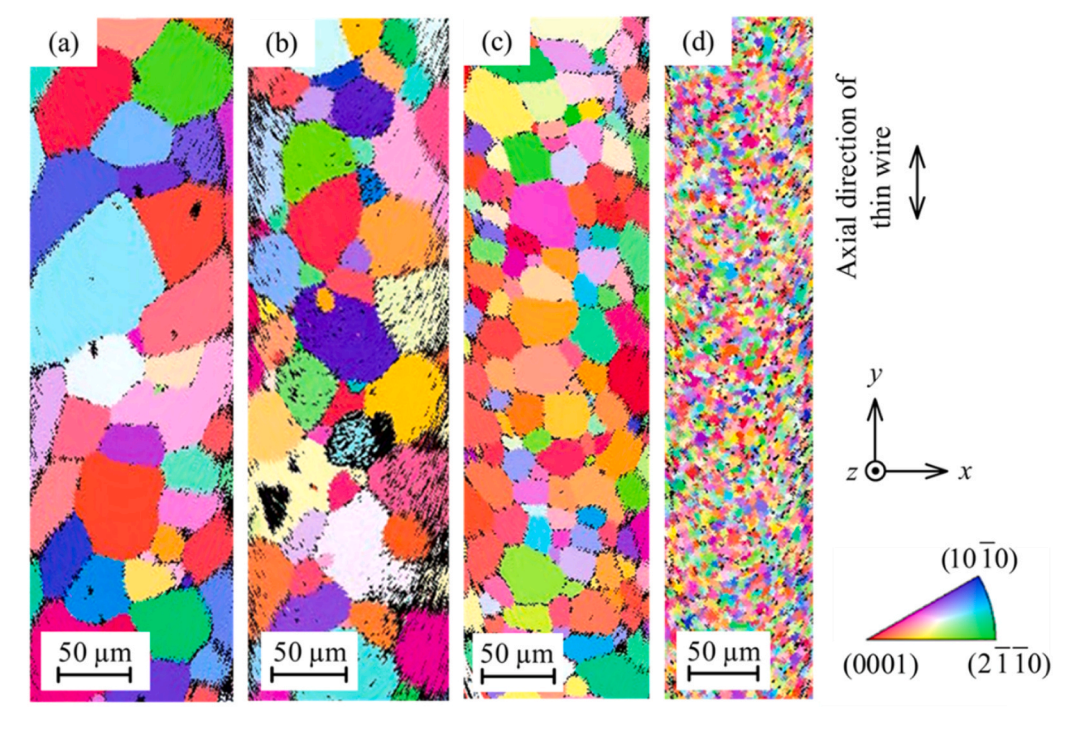


Fig. 2. IPF maps from the z direction of specimens annealed at (a) 1143 K, 120 min, (b) 1043 K, 120 min, (c) 943 K, 10 min, and (d) 843 K, 120 min.

Table 3Annealing conditions, average grain sizes, and number of grains across diameter.

Temperature [K]	Holding time [min]	Average grain size, $d_{\rm ave}$ [µm] ($d_{\rm ave}$ /D)	Number of grains across diameter, n
1143	120	52 (0.29)	3.4
1043	120	37 (0.21)	4.8
943	10	23 (0.13)	7.7
843	120	3.8 (0.02)	50

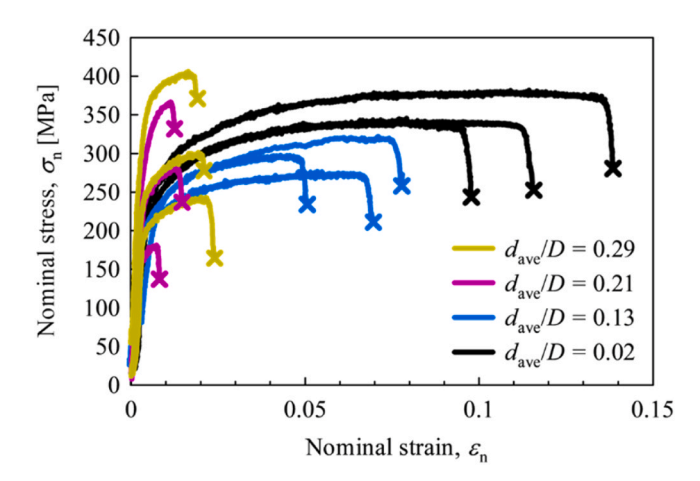


Fig. 3. Nominal stress-nominal strain curves of specimens.

orientations on the specimen surface obtained by EBSD before the tests.

3. Results

3.1. Microstructure

The corrected inverse pole figure (IPF) maps of the specimens in the z direction are shown in Fig. 2. As listed in Table 3, the values of $d_{\rm ave}$ of the

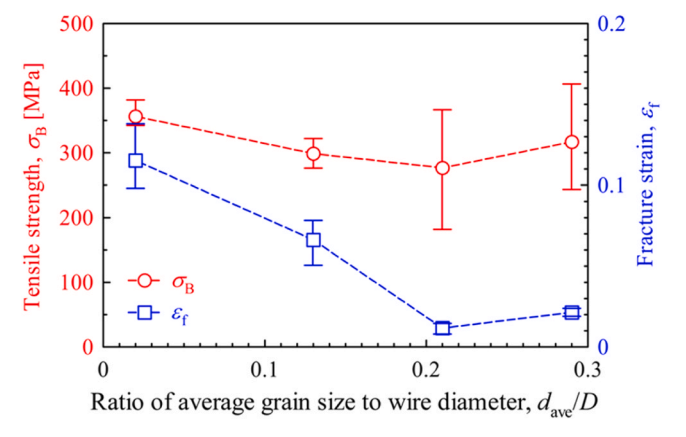


Fig. 4. Tensile strength and fracture strain at each $d_{\rm ave}/D$ ratio.

specimens annealed at 1143, 1043, 943, and 843 K were 52, 37, 23, and 3.8 μ m, respectively. The $d_{\rm ave}/D$ values for the different specimens were 0.29, 0.21, 0.13, and 0.02, respectively, which were used as the specimen names in this study. The n (= $D/d_{\rm ave}$) was 3.4, 4.8, 7.7, and 50, respectively.

3.2. Tensile tests

Fig. 3 shows the nominal stress-nominal strain curves for all the specimens. The average values and ranges of tensile strength and fracture strain for the specimens at each $d_{\rm ave}/D$ ratio are shown in Fig. 4. As $d_{\rm ave}/D$ increases, the variation in tensile strength becomes greater and the fracture strain decreases. This tendency is particularly apparent between 0.13 and 0.21. Furthermore, although it is generally known from the Hall-Petch law that yield stress decreases as grain size increases, some specimens with larger grain sizes ($d_{\rm ave}/D=0.21$ and 0.29) exhibited tensile strengths greater than those of specimens with smaller grain sizes ($d_{\rm ave}/D=0.02$ and 0.13). The reasons for this are considered

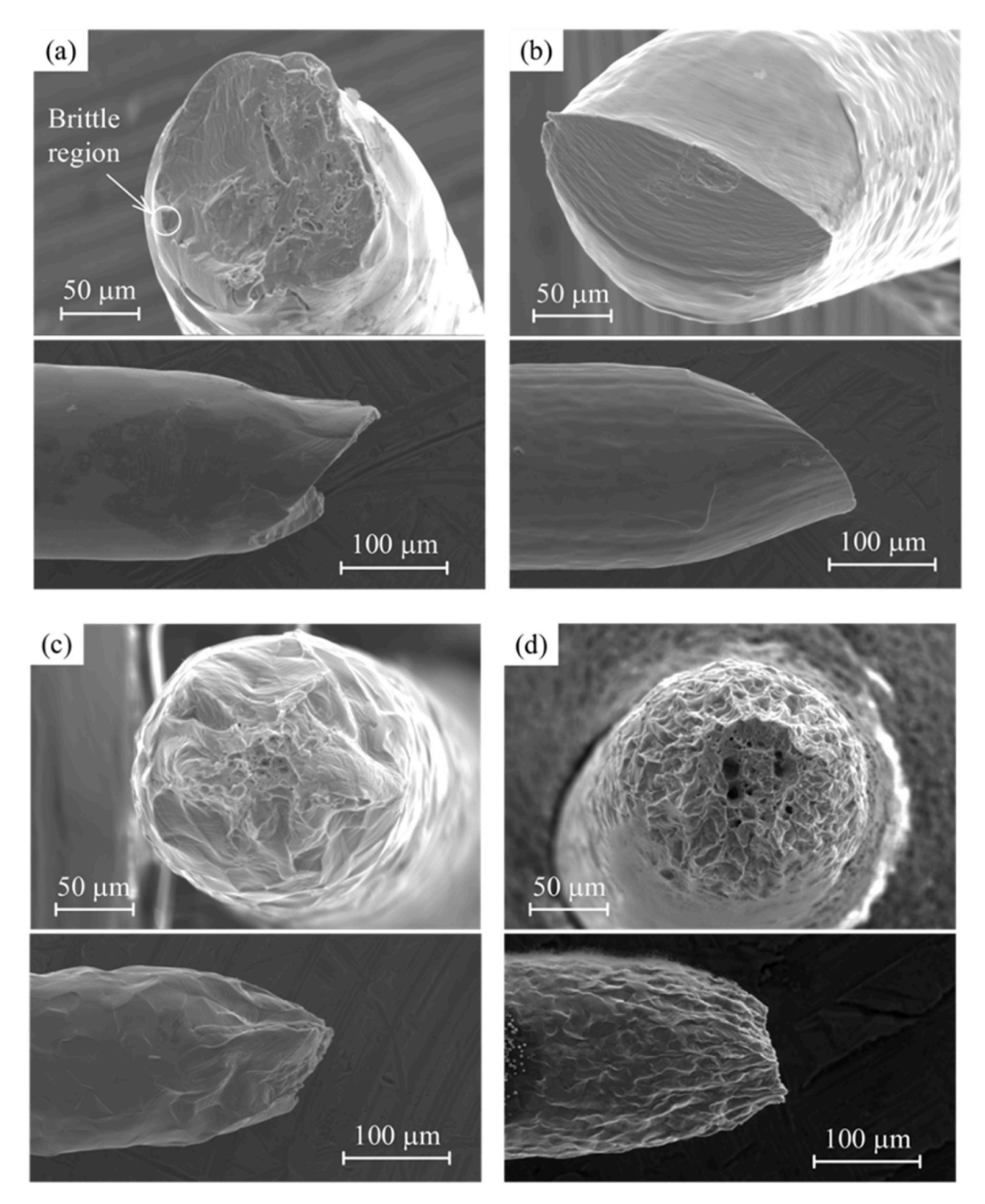


Fig. 5. Fracture surfaces from two different angles of specimens with $d_{\rm ave}/D$ of (a) 0.29, (b) 0.21, (c) 0.13, (d) 0.02.

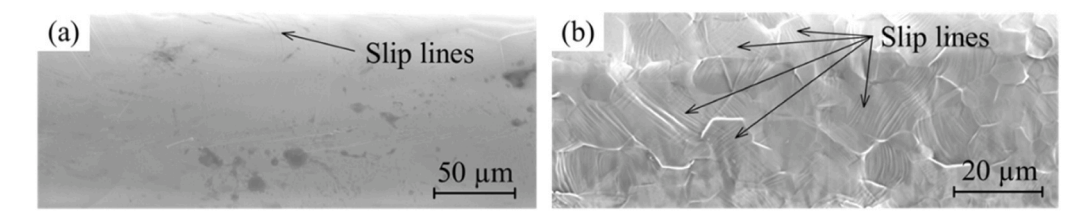


Fig. 6. Surfaces other than the fractured parts of specimens with $d_{\rm ave}/D$ of (a) 0.29 and (b) 0.02.

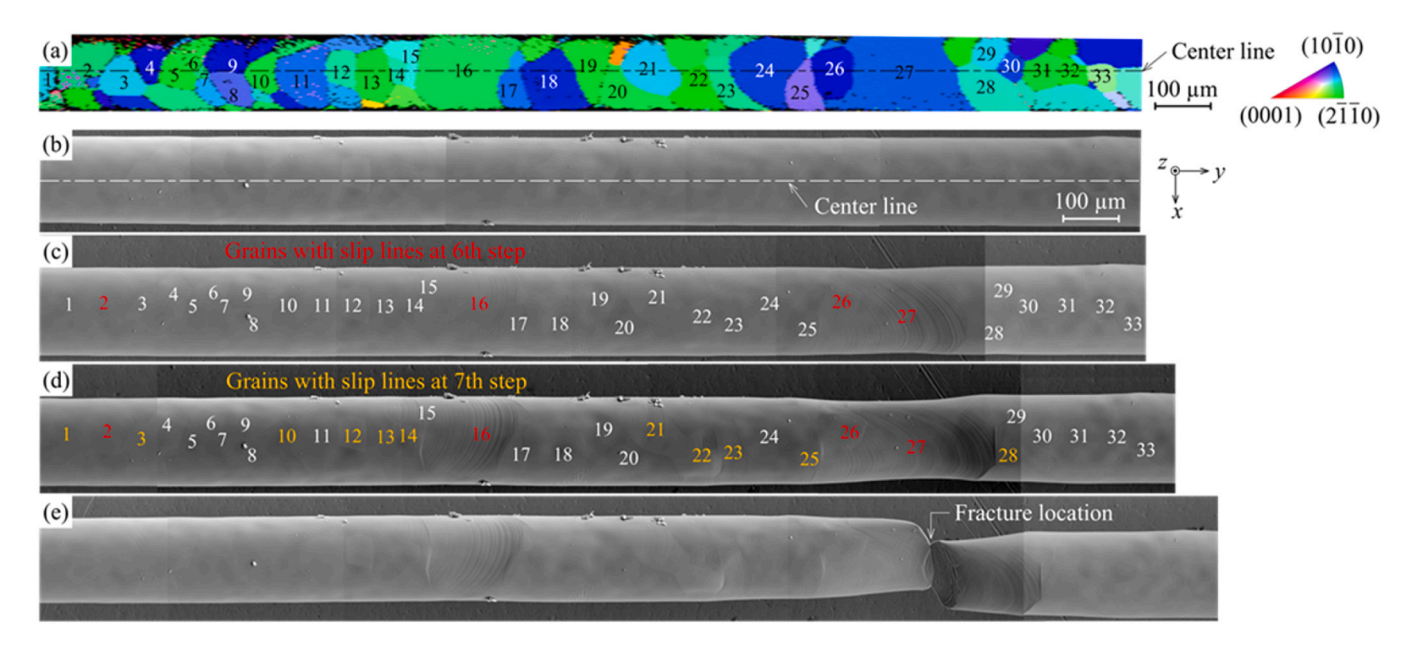


Fig. 7. (a) IPF map from the y direction and SEM images at the (b) 0th step, (c) 6th step, (d) 7th step, (e) 8th step of specimen with d_{ave}/D of 0.29 during the stepwise tensile test.

to be the increase in yield stress due to residual oxygen during hightemperature annealing [42] and the distribution of crystal orientations within the specimen, which will be discussed later.

Fig. 5 shows the fracture surfaces of the specimen captured from two different angles. For fracture surfaces with $d_{\rm ave}/D$ as small as 0.02 and 0.13, dimples were formed on the fracture surfaces almost perpendicular to the tensile direction, indicating cup-and-cone fracture. However, when d_{ave}/D was large (0.21 and 0.29), the fracture surface was inclined towards the tensile axis, with no clear dimples, and shear fracture occurred. Furthermore, in the case of $d_{ave}/D = 0.29$, which underwent heat treatment at the highest temperature, the most of the fracture surfaces were ductile, but some brittle fracture surfaces were observed. This is considered to be the brittle fracture surface observed in hightemperature heat-treated titanium alloys reported by Sirvin et al. [7]. Therefore, in the specimens annealed at high temperatures, oxygen ingress might be influencing the fracture morphology and macroscopic tensile properties. Fig. 6 shows SEM images captured from the z-direction other than the fracture part for $d_{ave}/D = 0.29$ and 0.02. In the case of $d_{ave}/D = 0.29$, there were only a few grains with slip lines and almost no surface roughening. However, when $d_{ave}/D = 0.02$, slip lines were seen in most grains and there was significant surface roughening. This suggests that when d_{ave}/D is large, almost no plastic deformation occurs other than at the fractured part, whereas when d_{ave}/D is small, plastic deformation occurs in regions other than the fractured part, which may determine the level of the fracture strain.

3.3. Stepwise tensile tests

Fig. 7 shows the IPF map from the y direction of the specimen with a $d_{\rm ave}/D$ of 0.29 and the SEM images of the specimen surfaces at different steps. As shown in Fig. 7(b), although the amount of electropolishing varied slightly for each grain, the grain boundaries were not deeply etched. The electropolishing generally provided a smooth surface finish. To investigate the effect of grain size, 33 grains along the center line in the figure were selected for evaluation to eliminate grains that were

partially visible. The number of grains is shown in the figure. Of the 33 grains, slip lines were first detected in four grains at the 6th step, and additional slip lines were identified in 11 grains at the 7th step. No slip lines were seen in the remaining 18 grains. In the part where the slip lines were detected at the 6th step, necking became larger at the 7th step, and fracture was observed at the 8th step. For each of the 15 grains with observed slip lines, the activated slip system was estimated on the basis of the angle of the slip line at the centerline of the specimen. As a result, it was revealed that the slip system with the highest MSF was activated in all 15 grains. Double slip was also observed in grains 25 and 26, and it was estimated that the slip system with the fourth and secondhighest MSF was activated in two grains with secondary slip activity. These two grains were located near the fractured part where the deformation was large, and it is assumed that multiple slips were caused by the deformation of the fractured part. All of the activated slip systems, including double slip, were prismatic <a> slip systems in all of the grains.

Fig. 8 shows the IPF map from the y direction of the specimen with a d_{ave}/D of 0.13 and the SEM images of the specimen surfaces at different steps. In this specimen, as in the specimen with a d_{ave}/D of 0.29, 34 grains along the centerline were targeted for evaluation. Of the 34 grains, slip lines were first detected in 12 grains at the 4th step, seven grains at the 5th step, and six grains by the 7th step. No slip lines were seen in the remaining nine grains. The ratio of the number of grains with slip lines before fracture was larger when d_{ave}/D was smaller. The MSF of the slip system activated in each grain is shown in Fig. 9 for the 25 grains for which the slip lines were identified. Consequently, 20 of the 25 grains (80 %) were estimated to have undergone slip deformation in the slip system with the highest MSF. They were all prismatic $\langle a \rangle$ slip systems. For the other five grains (grain nos. 4, 11, 13, 22, and 23), three different slip systems (One of the 1st pyramidal <a> slip systems and two of the 1st pyramidal <c+a> slip systems) were identified based on the angles of the surface slip lines observed in each grain. For each grain, the slip system with the highest MSF among these three was presumed to be activated. As a result, the pyramidal <a> slip system was presumed

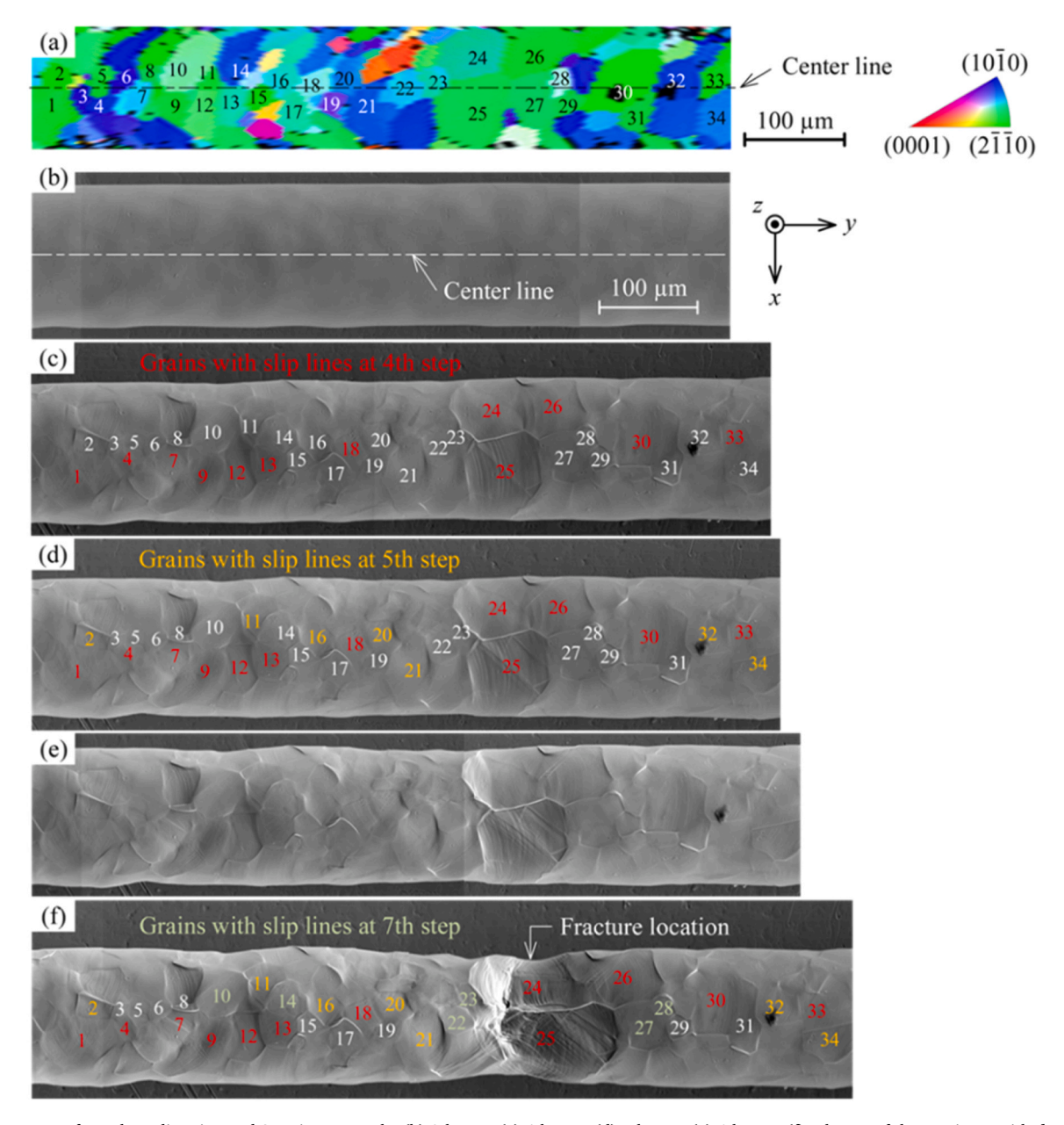


Fig. 8. (a) IPF map from the y direction and SEM images at the (b) 0th step, (c) 4th step, (d) 5th step, (e) 6th step, (f) 7th step of the specimen with d_{ave}/D of 0.13 during the stepwise tensile test.

to be activated in a relatively high MSF slip system (higher MSF than the 6th highest MSF) in all five grains. The values of m' and N were calculated for the four grains (grain nos. 11, 13, 22, and 23) for which slip lines were observed in the adjacent grains to determine whether slip was transferred from the adjacent grains. The results are presented in Tables 4, 5, 6, and 7. In the four grains, the m' and N values between the activated slip systems were not significantly large. Therefore, the geometrical slip plane and direction as well as the shear stress acting on the slip system were not similar for the two activated slip systems. The m' and N values with the grains inside the material are unknown, but if m' and N cannot explain the slip deformation of the four grains, the authors have two possible explanations. One possible explanation is that

the ease of slip deformation depends on the angle of the slip direction with respect to the free surface. Another is that when $d_{\rm ave}/D$ becomes somewhat small, it is geometrically necessary for the specimen as a whole to extend in the tensile direction (y direction), not only to deform in the same direction between adjacent grains, but also to deform in several directions in adjacent grains or in a single grain. Therefore, the activated slip system may have been subjected to higher shear stress than other slip systems.

Fig. 10 shows the timing of the slip line initiation in the grain size and *MSF* distribution diagram for each grain in the specimens with $d_{\rm ave}/D=0.29$ and 0.13, respectively. The grains in the fractured cross-section are indicated by arrows. For both specimens, there is no clear

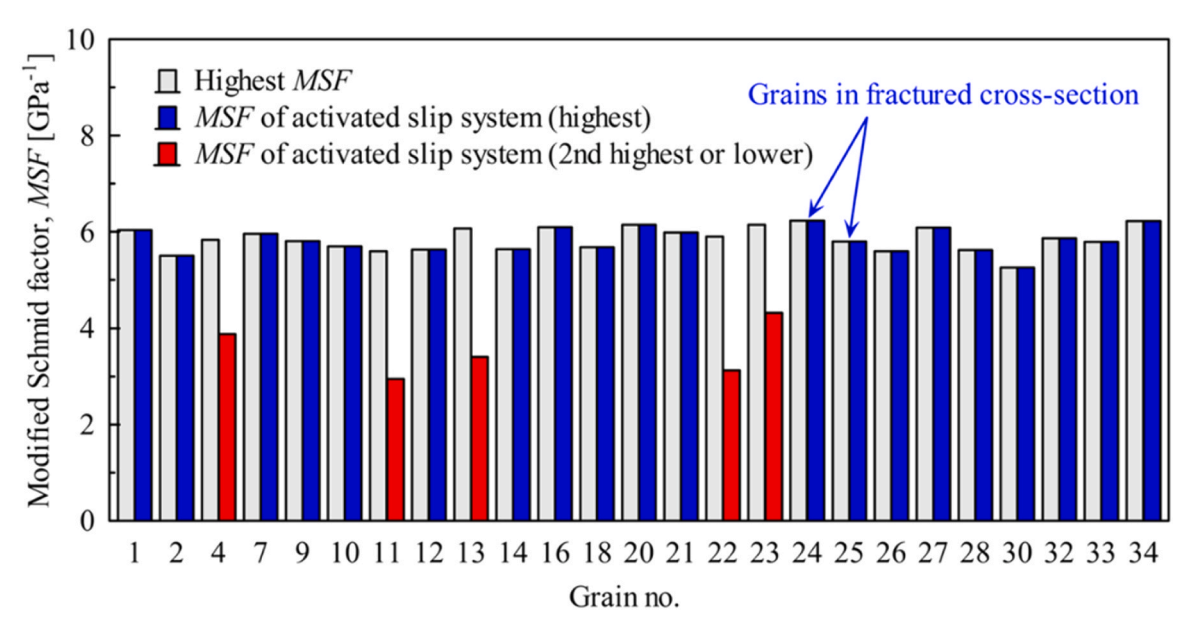


Fig. 9. *MSF* of activated slip system for each grain of specimen with $d_{\rm ave}/D$ of 0.13.

Table 4 m' parameters and N factors for slip systems of grain nos. 11 and 12.

Grain no. 11		Grain no. 12		m'	N	
Slip system ^a	MSF [GPa ⁻¹]	Slip system	MSF [GPa ⁻¹]			
(0110)[2110]	5.6 (Highest)	$(01\overline{1}0)[\overline{2}110]$	5.6 (Highest)	0.36	0.48	
$(1\overline{1}00)[\overline{1}\overline{1}20]$	5.0 (2nd highest)	Same as above		-0.05	0.14	
$(0\overline{1}11)[2\overline{1}\overline{1}0]$	3.9 (3rd highest)	Same as above		0.18	0.48	
$(1\overline{1}01)[\overline{11}20]$	3.5 (4th highest)	Same as above		-0.03	0.26	
$(01\overline{1}1)[\overline{2}110]$	3.3 (5th highest)	Same as above		0.45	0.36	
$(\overline{1}101)[11\overline{2}0]$	2.9 (6th highest)	Same as above		-0.06	-0.02	Activated

^a Slip system is presented using the Miller-Bravais index.

Table 5 m parameters and N factors for slip systems of grain nos. 13 and 14.

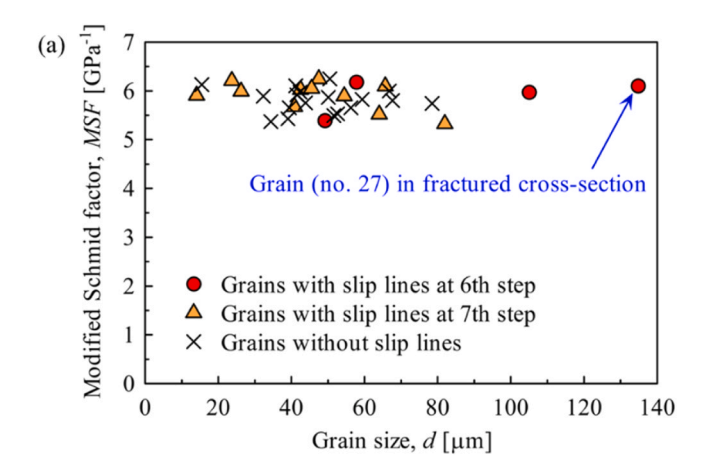
Grain no. 13		Grain no. 14		m'	N	
Slip system	MSF [GPa ⁻¹]	Slip system	MSF [GPa ⁻¹]			
(0110)[2110]	6.1 (Highest)	$(01\overline{1}0)[\overline{2}110]$	5.6 (Highest)	0.80	0.80	_
$(01\overline{1}1)[\overline{2}110]$	4.4 (2nd highest)	Same as above		0.99	0.99	
$(0\overline{1}11)[2\overline{1}\overline{1}0]$	3.4 (3rd highest)	Same as above		0.42	0.42	Activated

Table 6 m' parameters and N factors for slip systems of grain nos. 22 and 21.

Grain no. 22		Grain no. 21		m'	N	
Slip system	MSF [GPa ⁻¹]	Slip system	MSF [GPa ⁻¹]			
(1100)[1120]	5.9 (Highest)	$(01\overline{1}0)[\overline{2}110]$	6.0 (Highest)	0.00	0.88	
$(1\overline{1}01)[\overline{1}\overline{1}20]$	4.4 (2nd highest)	Same as above		-0.01	0.95	
$(01\overline{1}0)[\overline{2}110]$	3.4 (3rd highest)	Same as above		0.64	0.42	
$(\overline{1}101)[11\overline{2}0]$	3.1 (4th highest)	Same as above		0.01	0.59	Activated

Table 7 m parameters and N factors for slip systems of grain nos. 23 and 25.

Grain no. 23		Grain no. 25		m'	N	
Slip system	MSF [GPa ⁻¹]	Slip system	MSF [GPa ⁻¹]			
$(1\overline{1}00)[\overline{11}20]$	6.1 (Highest)	$(01\overline{1}0)[\overline{2}110]$	5.8 (Highest)	0.00	0.84	
$(1\overline{1}01)[\overline{1}\overline{1}20]$	4.3 (2nd highest)	Same as above		0.00	0.55	Activated



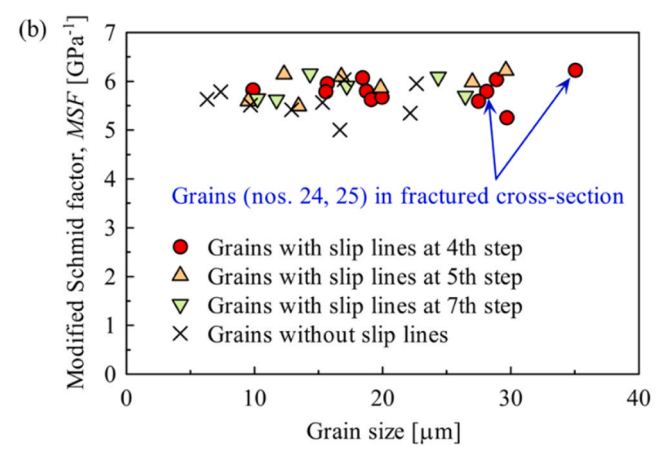


Fig. 10. Relationships between *MSF* and grain size. (a) $d_{\rm ave}/D=0.29$, (b) $d_{\rm ave}/D=0.13$.

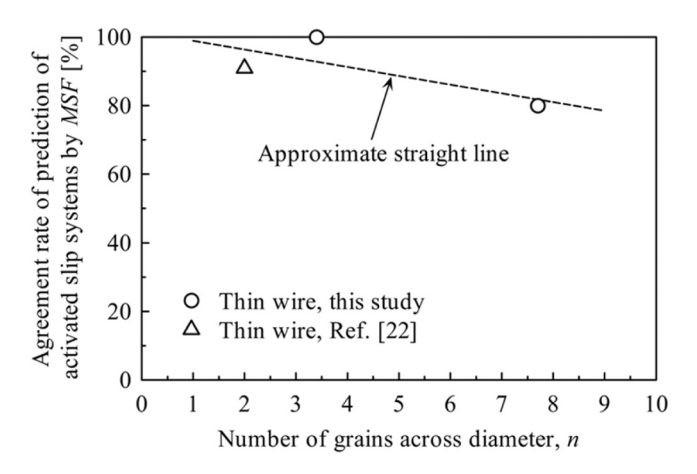
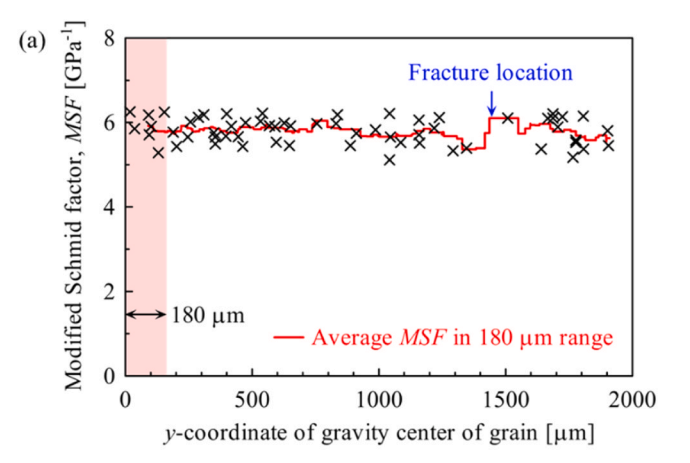


Fig. 11. Relationship between agreement rate of prediction of activated slip systems by *MSF* and number of grains across diameter.

relationship between the grain size, *MSF*, and slip line initiation. However, the fracture location was in the cross-section where large grains existed, and slip lines were observed in these grains at an early step.



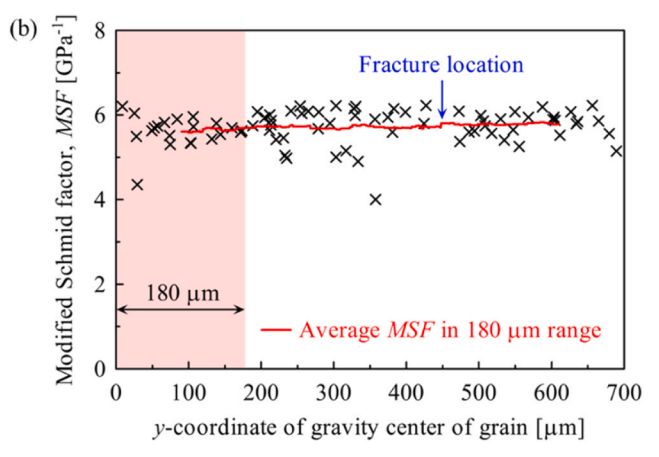
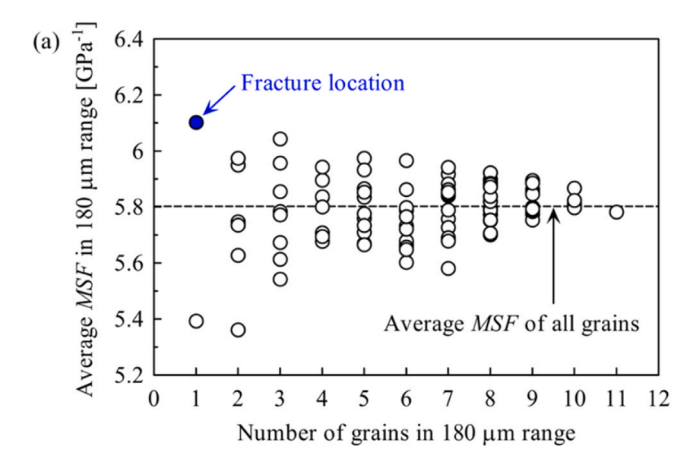


Fig. 12. Relationship between the *MSF* and *y*-coordinate of the gravity center of grain. (a) $d_{\rm ave}/D=0.29$, (b) $d_{\rm ave}/D=0.13$.

4. Discussion

4.1. Activated slip system in one grain of thin wire

Fig. 11 shows the relationship between the agreement rate of the prediction of the activated slip system by the highest MSF and the number of grains across the diameter in a pure titanium thin wire. The results of our previous study [22] and the approximate straight line are also presented. The results indicate that the prediction agreement rate tends to increase as n decreases. This is because when n is small, the cross-section is close to a single-crystal state, and the prediction agreement rate approaches 100 %. As n increases, the stress field becomes inhomogeneous in the cross-section owing to its relationship with other grains and is affected by the deformation of neighboring grains, which is thought to decrease the prediction agreement rate. The authors' group also predicted active slip systems near notches in pure titanium thin films [43]. In the case of the notch specimens, there are regions where the tensile and principal stress directions do not coincide. Therefore, a parameter called the slip activity (SA) was used to account for this. Activated slip systems were predicted for 87 % of the grains in the semicircular notch and 79 % of the grains in the semielliptical notch. In the plate material, there are many grains in the cross-section, and the interaction between the grains is considered to be larger than that in the thin wire. Therefore, even if *n* is large and the influence of neighboring



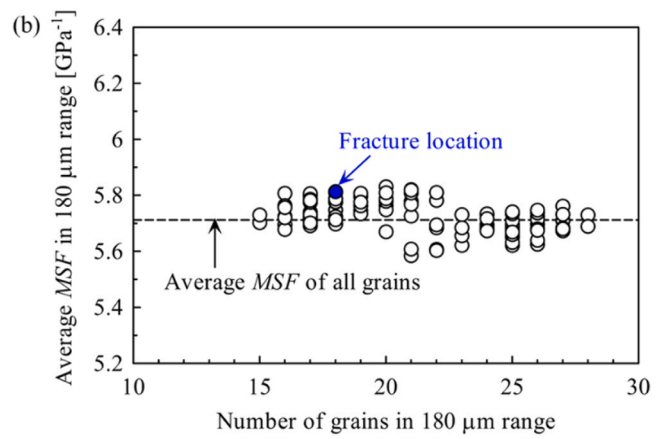


Fig. 13. Relationship between average MSF and number of grains in the 180 μ m range. (a) $d_{ave}/D=0.29$, (b) $d_{ave}/D=0.13$.

grains exists, approximately 80 % of the grains are considered to have active slip system that is most prone to slip deformation in the grain.

4.2. Fracture location in thin wire

Fig. 10 suggests that there is no clear relationship between d and MSF, and slip line initiation. However, the fracture locations, i.e., the location where deformation is likely to continue, might be affected by d. The reason for this is discussed introducing the parameter, the average MSF of the grains in the cross-section. In Fig. 12, the highest MSF of each grain is plotted at the y-coordinate of the gravity center of grain in the specimens with $d_{ave}/D = 0.29$ and 0.13. The average MSF of the grains in the 180 µm region in y direction is shown by the red line as the average MSF for each cross-section. The length is 180 µm, which is the same as the wire diameter because this region is considered to be involved in the deformation when shear fracture occurs at an angle of 45° to the tensile direction. It can be observed that the average MSF is higher at the fracture location where large grains are present. This suggests that the ease of deformation of a cross-section, and thus the ease of slip deformation of each grain depends not only on the MSF value of individual grains, but also on the average MSF value of the grains in the crosssection. The relationship between n and the average MSF in specimens

with $d_{ave}/D = 0.29$ and 0.13 is shown in Fig. 13. It is evident that as n increases, the average MSF becomes closer to the average value for all the grains, and the variance decreases. In other words, a cross-section with fewer grains has a larger variance, depending on the MSF of the fewer grains. Therefore, a cross-section with relatively large grains is likely to have the highest average MSF because the number of grains in the cross-section is small, and the variance is large. Such a cross-section with a high average MSF is considered to be more prone to slip deformation than other cross-sections, as shown in Fig. 14(a). Even after slip deformation, the cross-section is considered to have fewer grain boundaries and a higher fraction of grains facing the free surface, resulting in less work hardening and continued slip deformation, which is more likely to lead to shear fracture. Therefore, when d_{ave}/D is large, in addition to the decrease in flow stress due to Hall-Petch's law [23,24] and the decrease in work hardening of the entire specimen [15–17], the variance of the average MSF for each cross-section increases, and the location where slip deformation occurs becomes localized, resulting in a decrease in fracture strain as shown in Fig. 4. In addition, as d_{ave}/D increases, the number of grains in the specimen decreases, leading to differences in the grain size and crystal orientation of each specimen, which is considered to cause variations in the tensile strength shown in Fig. 4. As illustrated in Fig. 14(b), when d_{ave}/D is small, the average MSF values of the cross-sections are almost the same. In addition, a grain boundary density increases and a surface grain fraction decreases, resulting in easier work hardening. This is likely to result in uniform deformation as shown in Fig. 14(b).

5. Conclusions

In this study, tensile and stepwise tensile tests were conducted on specimens with different average grain sizes to clarify the effects of the grain size and crystal orientation on the tensile properties of pure titanium thin wires. The main conclusions are as follows:

- (1) When the grain size was large, the fracture strain was significantly smaller and the variation in tensile strength was larger. The grain-size threshold for such properties was considered to be the grain-size ratio with a wire diameter of 0.13 or greater. This is because when the grain size is larger, the variance of the average MSF for each cross-section increases and the location where slip deformation occurs becomes localized, resulting in a decrease in fracture strain. In addition, the number of grains in the specimen decreases, leading to differences in the grain size and crystal orientation of each specimen, which is considered to cause variations in the tensile strength.
- (2) For larger grain sizes, the percentage of activation of slip systems with the highest MSF for each grain was higher (15/15 = 100 %), whereas for smaller grain sizes, the percentage was lower (20/25 = 80 %). This may be because the larger grain is similar to the single-crystal state and the smaller grain is more affected by intergrain constraints.
- (3) For larger grain sizes, the fracture location in a thin wire was highly correlated with the average MSF of the grains in the crosssection. Furthermore, a cross-section with relatively large grains is likely to have the highest average MSF because the number of grains in the cross-section is small, and the variance is large.

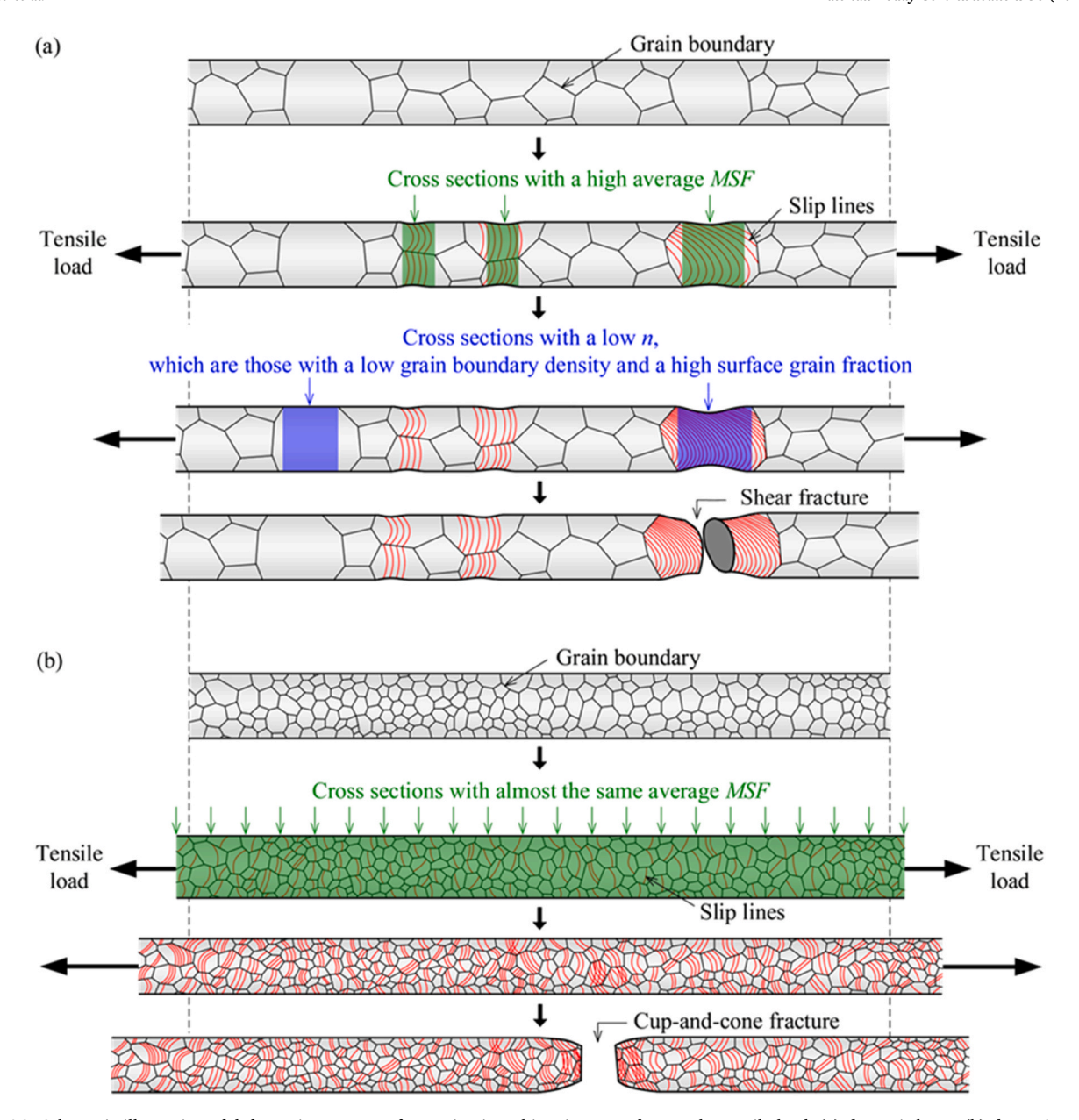


Fig. 14. Schematic illustration of deformation process of pure titanium thin wire up to fracture by tensile load. (a) d_{ave}/D is large, (b) d_{ave}/D is small.

CRediT authorship contribution statement

Naoya Tada: Writing – review & editing, Supervision, Resources, Project administration, Funding acquisition, Formal analysis, Conceptualization. Takeshi Uemori: Writing – review & editing, Formal analysis. Junji Sakamoto: Writing – original draft, Visualization, Methodology, Investigation, Formal analysis.

Funding

This study was supported by JSPS KAKENHI [grant number JP21H01214].

Declaration of Competing Interest

The authors declare that they have no known competing financial interests or personal relationships that could have appeared to influence the work reported in this paper.

Acknowledgments

The authors are grateful to Kota Tanaka for his support during the tests. We also would like to thank Editage (www.editage.jp) for English language editing.

Data Availability

Data will be made available on request.

References

- C. Leyens, M. Peters, Titanium and Titanium Alloys: Fundamentals and Applications, Wiley-VCH Press, Weinheim, 2003.
- [2] T. Narushima, Titanium and its alloys as biomaterials, J. Jpn. Inst. Light Met. 55 (2005) 561–565, https://doi.org/10.2464/jilm.55.561.
- [3] A.W. Thompson, Use of non-polycrystal specimens in mechanical behavior tests, Scr. Met. 8 (1974) 145–147, https://doi.org/10.1016/0036-9748(74)90461-X.
- [4] S. Miyazaki, K. Shibata, H. Fujita, Effect of specimen thickness on mechanical properties of polycrystalline aggregates with various grain sizes, Acta Met. 27

- (1979) 855-862, https://doi.org/10.1016/0001-6160(79)90120-2 (Get rights and
- C. Keller, E. Hug, Hall-Petch behaviour of Ni polycrystals with a few grains per thickness, Mater. Lett. 62 (2008) 1718-1720, https://doi.org/10.1016/j
- [6] D. Texier, J. Genée, V. Velay, A.C. Moreno, D. Monceau, E. Andrieu, Size effects on the plastic behavior of polycrystalline materials: grain size, precipitation state and free-surface effects, Int. J. Plast. 188 (2025) 104284, https://doi.org/10.1016/j.
- [7] Q. Sirvin, J. Genee, B. Dod, D. Monceau, D. Texier, Oxygen ingress in titanium and its alloys after high-temperature oxidation: a competition between strengthening and embrittlement, Metall. Mater. Trans. A. 56 (2025) 1858-1874, https://doi. org/10.1007/s11661-025-07737-0.
- [8] C. Zhu, J. Xu, H. Yu, D. Shan, B. Guo, Size effect on the high strain rate micro/ meso-tensile behaviors of pure titanium foil, J. Mater. Res. Technol. 11 (2021) 2146-2159, https://doi.org/10.1016/j.jmrt.2021.02.022
- [9] S. Wang, L. Niu, C. Chen, Y. Pang, B. Liao, Z.H. Zhong, P. Lu, P. Li, X.D. Wu, J. W. Coenen, L.F. Cao, Y.C. Wu, Size effects on the tensile properties and deformation mechanism of commercial pure titanium foils, Mater. Sci. Eng. A. 730 (2018) 244-261, https://doi.org/10.1016/j.msea.2018.06.009.
- [10] X.F. Tang, L.F. Peng, S.Q. Shi, M.W. Fu, Influence of crystal structure on size dependent deformation behavior and strain heterogeneity in micro-scale deformation, Int. J. Plast. 118 (2019) 147-172, https://doi.org/10.1016/j
- [11] L. Sun, Z. Xu, L. Peng, X. Lai, Effect of grain size on the ductile-brittle fracture behavior of commercially pure titanium sheet metals, Mater. Sci. Eng. A. 822 (2021) 141630, https://doi.org/10.1016/j.msea.2021.14163
- [12] L. Sun, Z. Xu, L. Peng, X. Lai, Grain-size-dependent ductile-to-brittle fracture mechanism of titanium sheets, Scr. Mater. 219 (2022) 114877, https://doi.org/ 10.1016/j.scriptamat.2022.114877.
- L. Sun, H. Yang, Z. Xu, M.M. Shahzamanian, D. Qiu, L. Peng, X. Lai, M.W. Fu, Unraveling the co-evolution of microstructure and damage in α -titanium, Int. J. Mech. Sci. 291-292 (2025) 110161, https://doi.org/10.1016/j. ijmecsci.2025.110161.
- [14] J. Yang, P. Han, F. Yang, H. Chi, Z. Cheng, X. Wang, Revealing the mechanism of size effect on the forming limit of TA1 pure titanium foil at micro/meso scale through microstructure evolution, J. Alloy. Compd. 1040 (2025) 183706, https:// doi.org/10.1016/j.iallcom.2025.183706.
- [15] T. Fukumaru, H. Hidaka, T. Tsuchiyama, S. Takaki, Effect of wire diameter and grain size on tensile properties of austenitic stainless steel wire (in Japanese), TetsuToHagane 91 (2005) 828-833, https://doi.org/10.2355/ tetsutohagane1955.91.11_828.
- S. Fu, D. Yu, Y. Chen, K. An, X. Chen, Size effect in stainless steel thin wires under tension, Mater. Sci. Eng. A. 790 (2020) 139686, https://doi.org/10.1016/j
- [17] C. Wang, C. Wang, B. Guo, D. Shan, G. Huang, Size effect on flow stress in uniaxial compression of pure nickel cylinders with a few grains across thickness, Mater. Lett. 106 (2013) 294-296, https://doi.org/10.1016/j.matlet.2013.05.037.
- C. Wang, C. Wang, J. Xu, P. Zhang, D. Shan, B. Guo, Plastic deformation size effects in micro-compression of pure nickel with a few grains across diameter, Mater, Sci. Eng. A. 636 (2015) 352-360, https://doi.org/10.1016/j.msea.2015.03.087
- [19] C. Wang, C. Wang, J. Xu, P. Zhang, D. Shan, B. Guo, Z. Wang, Tensile deformation behaviors of pure nickel fine wire with a few grains across diameter, Trans. Nonferrous Met. Soc. China 26 (2016) 1765-1774, https://doi.org/10.1016/ \$1003-6326(16)64287-5
- [20] X.X. Chen, A.H.W. Ngan, Specimen size and grain size effects on tensile strength of Ag microwires, Scr. Mater. 64 (2011) 717-720, https://doi.org/10.1016/j. rintamat 2010 12 031.
- [21] X.X. Chen, A.H.W. Ngan, Tensile deformation of silver micro-wires of small thickness-to-grain-size ratios, Mater. Sci. Eng. A. 539 (2012) 74-84, https://doi. rg/10.1016/j.msea.2012.01.054.
- [22] J. Sakamoto, N. Tada, T. Uemori, Tensile properties and slip deformation behavior of pure titanium thin wire with a small diameter-to-grain-size ratio, Mater. Sci. Eng. A. 863 (2023) 144532, https://doi.org/10.1016/j.msea.2022.144532
- E.O. Hall, The deformation and ageing of mild steel: III discussion of results, Proc.
- Phys. Soc. B. 64 (1951) 747–753, https://doi.org/10.1088/0370-1301/64/9/303. N.J. Petch, The cleavage strength of polycrystals, J. Iron Steel Inst. 174 (1953)

- [25] Y. Kawano, T. Mayama, M. Mitsuhara, Formation of plate-like high-strain region in polycrystalline α-titanium and its relation to high-strain bands on surface, Mater. Today Commun. 39 (2024) 109230, https://doi.org/10.1016/ mtcomm.2024.109230
- [26] Y. Kawano, M. Sato, T. Mayama, M. Mitsuhara, S. Yamasaki, Quantitative evaluation of slip activity in polycrystalline α-titanium considering non-local interactions between crystal grains, Int. J. Plast. 127 (2020) 102638, https://doi. org/10.1016/j.ijplas.2019.12.001.
- [27] Y. Kawano, T. Mayama, T. Okamoto, M. Mitsuhara, Local slip activities in polycrystalline α-Ti depending on textures and strain rates, Mater. Sci. Eng. A. 843 (2022) 143133, http /doi.org/10.1016/j.msea.2022.14313
- Y. Niu, Y. Jia, X. Lv, Y. Zhu, Y. Wang, Molecular dynamics simulations of the effect of gradient grain size on the mechanical properties of polycrystalline titanium, Mater. Today Commun. 45 (2025) 112457, https://doi.org/10.1016/j.
- [29] C. Ma, L. Shen, S. Yang, Z. Li, Y. Cheng, L. Zhao, X. Guo, Mechanical behavior and deformation mechanisms of rolled commercially pure titanium sheet under tensile loading after pre-deformation, J. Alloy. Compd. 1037 (2025) 182497, https://doi. .iallcom.2025.18249
- [30] H. Zhang, J. Xu, Y. Tan, Y. Bao, X. Ji, W. Zeng, H. Li, Research on the texture evolution characteristics and intrinsic mechanisms of pure titanium thin plate during in situ tensile testing of different directions, J. Alloy. Compd. 1042 (2025) /doi.org/10.1016/j.jallcom.2025.1841
- [31] X. Ji, J. Xu, H. Zhang, J. Du, W. Zeng, W. Wang, Plastic deformation mechanism of TA1 pure titanium plate using SEM-EBSD in-situ tensile testing, Mater. Sci. Eng. A. 908 (2024) 146768, https://doi.org/10.1016/j.msea.2024.146768.
- [32] B. Wang, Z. Xiang, Z. Zhou, J. Chen, C. Qian, Z. Chen, Effect of microstructure and texture on mechanical properties of TA1 pure titanium sheets in different rolling processes, Mater. Today Commun. 46 (2025) 112560, https://doi.org/10.1016/j. mtcomm,2025,112560.
- [33] J.L.W. Warwick, N.G. Jones, K.M. Rahman, D. Dye, Lattice strain evolution during tensile and compressive loading of CP Ti, Acta Mater. 60 (2012) 6720-6731, https://doi.org/10.1016/j.actamat.2012.08.042
- [34] A.A. Salem, S.R. Kalidindi, S.L. Semiatin, Strain hardening due to deformation twinning in α-titanium: constitutive relations and crystal-plasticity modeling, Acta Mater. 53 (2005) 3495–3502, https://doi.org/10.1016/j.actamat.2005.04.014.
- [35] X. Wu, S.R. Kalidindi, C. Necker, A.A. Salem, Prediction of crystallographic texture evolution and anisotropic stress-strain curves during large plastic strains in high purity α -titanium using a Taylor-type crystal plasticity model, Acta Mater. 55 (2007) 423–432, https://doi.org/10.1016/j.actamat.2006.08.034.
- K.E.K. Amouzou, T. Richeton, A. Roth, M.A. Lebyodkin, T.A. Lebedkina, Micromechanical modeling of hardening mechanisms in commercially pure α-titanium in tensile condition, Int. J. Plast. 80 (2016) 222-240, https://doi.org/ 10.1016/i.iiplas.2015.09.008.
- [37] L. Wang, R.I. Barabash, Y. Yang, T.R. Bieler, M.A. Crimp, P. Eisenlohr, W. Liu, G. E. Ice. Experimental characterization and crystal plasticity modeling of heterogeneous deformation in polycrystalline α-Ti, Metall. Mater. Trans. A. 42 (2011) 626-635, https://doi.org/10.1007/s11661-010-0249-8.
- L. Wang, Z. Zheng, H. Phukan, P. Kenesei, J.S. Park, J. Lind, R.M. Suter, T.R. Bieler, Direct measurement of critical resolved shear stress of prismatic and basal slip in polycrystalline Ti using high energy X-ray diffraction microscopy, Acta Mater. 132 (2017) 598-610, https://doi.org/10.1016/j.actamat.2017.05.015
- [39] J. Gong, A.J. Wilkinson, Anisotropy in the plastic flow properties of single-crystal $\boldsymbol{\alpha}$ titanium determined from micro-cantilever beams, Acta Mater. 57 (2009) 5693-5705, https://doi.org/10.1016/j.actamat.2009.07.064.
- J. Luster, M.A. Morris, Compatibility of deformation in two-phase Ti-Al alloys: dependence on microstructure and orientation relationships, Metall. Mater. Trans. A. 26 (1995) 1745–1756, https://doi.org/10.1007/BF02670762
- J.D. Livingston, B. Chalmers, Multiple slip in bicrystal deformation, Acta Met. 5 (1957) 322-327, https://doi.org/10.1016/0001-6160(57)90044-
- [42] F. Amann, R. Poulain, S. Delannoy, J.P. Couzinié, E. Clouet, I. Guillot, F. Prima, An improved combination of tensile strength and ductility in titanium alloys via oxygen ordering, Mater. Sci. Eng. A. 867 (2023) 144720, https://doi.org/10.1016/
- [43] N. Tada, T. Uemori, J. Sakamoto, Prediction of slip activity of crystal grains around semi-circular and semi-elliptical notches in thin-sheet specimens of pure titanium using formulated macroscopic stress distribution and crystal orientation, Eng. Fail. Anal. 153 (2023) 107623, https://doi.org/10.1016/j.engfailanal.2023.107